Case Studies in Thermal Engineering 28 (2021) 101394

Contents lists available at ScienceDirect

Case Studies in Thermal Engineering

journal homepage: www.elsevier.com/locate/csite

MHD natural convection nanofluid flow in a heat exchanger: Effects of Brownian motion and thermophoresis for nanoparticles distribution

Yan Cao [a], Hamdi Ayed [b], Fahd Jarad [c,d,**], Hussein Togun [e,f,***], Hajar Alias [e], Alibek Issakhov [g], Mahidzal Dahari [h], Makatar Wae-hayee [i,*], Mohamed Hechmi El Ouni [b]

[a] School of Mechatronic Engineering, Xi'an Technological University, Xi'an, 710021, China
[b] Department of Civil Engineering, College of Engineering, King Khalid University, Abha, 61421, Saudi Arabia
[c] Department of Mathematics, Cankaya University, Etimesgut, 06790, Ankara, Turkey
[d] Department of Medical Research, China Medical University, Taichung, 40402, Taiwan
[e] School of Chemical and Energy Engineering, Faculty of Engineering, University Teknologi Malaysia, 81310, UTM Johor, Bahru, Malaysia
[f] Biomedical Engineering Department, University of Thi-Qar, 64001, Nassiriya, Iraq
[g] Department of Mathematical and Computer Modelling, al -Farabi Kazakh National University, 050040, Almaty, Kazakhstan
[h] Department of Electrical Engineering, Faculty of Engineering, University Malaya, 50603, Kuala Lumpur, Malaysia
[i] Department of Mechanical and Mechatronics Engineering, Faculty of Engineering, Prince of Songkla University, Hatyai, Songkhla, 90110, Thailand

ARTICLE INFO

Keywords:
Buongiorno model
MHD
Heat exchanger
Heater/cooler
Natural convection
Cu nanoparticles

ABSTRACT

The free convection of Cu-water nanofluid is simulated and investigated inside a square heat exchanger chamber in the presence of MHD magnetic field. The Buongiorno model with the effects of Brownian and thermophoresis motion is considered to nanoparticles distribution inside the chamber. The geometry consists of a square chamber with two cylinders on the right and left sides as heater and cooler in order to create the buoyancy force, respectively. These cylinders represent hot and cold pipes, and the walls of the chamber are heat and mass insulation. the FVM with SIMPLE algorithm are used for velocity and pressure coupling. In current two-phase simulation, the effects of Rayleigh number, Hartmann number, inclination angle of chamber and volume fraction on streamline contours, isothermal lines, Lorentz force lines, nanoparticle distribution and Nusselt number are investigated. By modeling the motion of nanoparticles and evaluating it, a nanoparticle transport zone was observed. The diffusion effects of thermophoresis were significant in this zone. The nanoparticles were thrown from the hot cylinder to the cold cylinder. The application of a magnetic field enlarged the nanoparticle transport zone. However, increasing the Rayleigh number and decreasing the inclination angle of the enclosure caused the nanoparticles to disperse evenly.

* Corresponding author.
** Corresponding author. Department of Mathematics, Cankaya University, Etimesgut 06790, Ankara, Turkey.
** Corresponding author. School of Chemical and Energy Engineering, Faculty of Engineering, University Teknologi Malaysia, 81310 UTM Johor Bahru, Malaysia.
E-mail addresses: fahd@cankaya.edu.tr (F. Jarad), htokan_2004@yahoo.com (H. Togun), wmakatar@eng.psu.ac.th (M. Wae-hayee), melouni@kku.edu.sa (M.H. El Ouni).

https://doi.org/10.1016/j.csite.2021.101394
Received 7 August 2021; Received in revised form 19 August 2021; Accepted 25 August 2021
Available online 1 September 2021

1. Introduction

The natural convection inside the chambers and the control of the flow characteristics and the nanoparticles have many applications in the field of environment, agriculture, renewable energy, and industrial processes [1–6]. The use of the natural convection for heat exchangers is one of the most applications in industrial processes. Garoosi et al. [7] investigated the free convection of three types of nanoparticles inside a chamber with different number and arrangement of heaters and coolers (HACs). They applied Cu, Al_2O_3, and TiO_2 nanoparticles with homogeneous model for nanofluid. The whose results show that in all Rayleigh numbers, increasing the pairs number of HACs is more efficient than increasing the size of the HACs. Also, in low Rayleigh numbers, increasing the volume fraction enhances the Nusselt number, but in high Rayleigh numbers, the optimal volume fraction of nanoparticles is 1%. Heat exchangers are

Nomenclature

B_0	Uniform magnetic flux density, [T]
C	Specific heat, [J kg^{-1} K^{-1}]
d	Diameter, [m]
D	Diffusion coefficient, [m^2 s^{-1}]
g	Gravitational acceleration, [m s^{-2}]
H	Characteristic length, [m]
L	Length of the cavity, [m]
k	Thermal conductivity, [W m^{-1} K^{-1}]
k_B	Boltzmann's constant (=1.38066 × 10^{-23}), [J K^{-1}]
P	Pressure, [N m^{-2}]
T	Temperature, [K]
V	Velocity vector, [m s^{-1}]
x, y	Cartesian coordinates, [m]

Greek symbols

α	Thermal diffusivity, [m^2 s^{-1}]
β	Thermal expansion coefficient, [K^{-1}]
δ	Dimensionless parameter
η	Inclination angle of enclosure, [−]
μ	Dynamic viscosity, [kg m^{-1} s^{-1}]
ν	Kinematic viscosity, [m^2 s^{-1}]
ρ	Density, [kg m^{-3}]
σ	Electrical conductivity, [$\Omega^{-1}m^{-1}$]
ϕ	Volume fraction, [−]
γ	Constant parameter

Dimensionless number

Ha	Hartmann number
Le	Lewis number
Nu	Nusselt number
N_{BT}	Ratio of Brownian to thermophoretic diffusivity
Pr	Prandtl number
Ra	Rayleigh number
Sc	Schmidt number

Subscript

Ave	Average
B	Brownian
C	Cold
f	Fluid
Loc	Local
H	Hot
nf	Nanofluid
np	Nanoparticle
m	Mean
T	Thermophoresis
*	Dimensionless unit

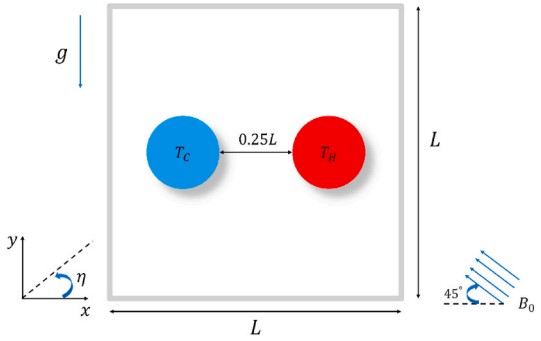

Fig. 1. The geometry of the problem consisting of a heater and a cooler in the presence of a uniform magnetic field.

used in a wide application in industries such as thermodynamic cycles, biomass, natural gas and oil storage and production [8–11]. Hence it has received diverse attention. In another study of Garoosi et al. [12], they also used cylindrical heaters and coolers inside square, circular and triangular chambers. They found that at Ra = 1e5, the heat transfer rate reduces with the addition of nanoparticles to the base fluid. On the other hand, the highest amount of heat transfer rate in a constant Rayleigh number occurs in a square, circular and triangular chamber, respectively.

With the development of industry and the growing energy issues, a proper understanding of heat transfer and areas related to improving related technology has become very important for researchers [13–16]. One of the effective techniques to overcome the concerns in this regard is using an external magnetic field and nanoparticles. Here are some studies and their results on the use of Magneto-Hydro-Dynamics (MHD) in free convection. Ahmed et al. [17] simulated the free convection of MHD inside a porous triangular chamber with a vertical fin and a block at the bottom of the chamber. They studied and changed block and fin height, temperature condition of block and fin, and the Hartmann number. The results predicted that the presence of a magnetic field would reduce the flow velocity and thus reduce the heat transfer rate. Massoudi et al. [18] numerically studied the free convection of MHD nanofluid water-diamonds inside a trapezoidal chamber and an elliptical cylinder in the center. They understood that increasing the Hartmann number reduces the transfer heat transfer rate.

One of the most important models of nanoparticle distribution in numerical simulations is the Buongiorno two-phase model [19]. Buongiorno pointed out that in laminar flows only the mechanisms of Brownian and thermophores diffusion are important. The Brownian and thermophoresis motion of the nanoparticles are due to the volume fraction gradient and the temperature gradient, respectively. Alhashash [20] simulated the natural convection of nanofluid with two phases model inside a porous chamber and a cylinder in the center. He showed that the heat transfer rate is directly related to the Darcy number and volume fraction. Sheikhzadeh et al. [21] showed that the two-phase model has more accurate results with experimental results by applying the Buongiorno two-phase model in the free convection of water-Al_2O_3. Also, the studies [22–25] investigated the free convection flow with two phases model. They showed that the density of nanoparticles distribution is directly related to increasing the temperature difference and decreasing the Rayleigh number. Moreover, Garoosi et al. [26] simulated the free convection of nanofluids with a two-phase model inside a cavity and different layouts of HACs. They concluded that HACs locations have a significant effect on heat transfer rate. Also, in low Rayleigh numbers, there is a non-uniform distribution of nanoparticles but in high Rayleigh numbers there is a uniform distribution.

The research [27,28] simulated the natural convection of water-Al2O3 nanofluid. They modeled the Buongiorno two-phase model for the distribution of nanoparticles inside an enclosure with a square solid in the center. Several number of other studies also investigated the natural convection of nanofluids under Lorentz force. Studies [29,30] simulated the nanoparticle distribution under MHD conditions using the Bongiorno two-phase model. Sheremet et al. [30] showed that an intensify in the magnetic field makes the decreasing rate of the average Nusselt number reduces.

In previous studies, free convection heat transfer in HAC configuration with water-Cu nanofluid in the two-phase model has not been investigated. Also, the parameters associated with the presence of the magnetic field, and the effects of MHD conditions have not been accurately evaluated.

In the present simulation, a uniform magnetic field and Buongiorno two-phase model are applied to MHD natural convection of Water-Cu nanofluid inside a cavity chamber with a pair of heater and a cooler. The cavity walls are heat and mass insulation, and Lorentz force is applied to the momentum equation. Also, the effects of nanoparticles mass flux are considered due to Brownian and thermophoresis mechanisms. This study focuses on the effects of Rayleigh, Hartmann number, volume fraction and inclination angle.

1.1. Problem description and geometry

In this study, we intend to take a small step in this area. The geometry of the heat exchanger consists of a heat and mass insulation cavity with length and height L, and two pipes with diameter of 0.25 L as a heater and cooler (Fig. 1). The surface temperatures of the right and left pipes are at the hot temperature T_H and the cold temperature T_C, respectively. These HACs creates the buoyancy force for natural convection inside the cavity [12and31]. On the other hand, a uniform magnetic field B_0 is embedded with a constant angle of

45° to the -x direction. the cavity is also deflectable with the η angle, and is filled with copper nanoparticles and water-based fluid.

1.2. Assumptions and equations

The MHD free convection of Cu-water nanofluid with Buongiorno model inside a chamber is simulated with **Assumptions**: steady, incompressible, Boussinesq approximation, two-dimensional, and Thermal equilibrium between the nanoparticles and the fluid [32]. Also, due to the presence of a uniform magnetic field, the MHD model has been used in momentum equations. On the other hand, the Buongiorno two-phase model is used to distribute copper nanoparticles and mass effects on the energy equation. By defining the appropriate dimensionless parameters and applying them to the equations, the dimensionless equations of continuity, momentum, energy and mass can be expressed as follows:

dimensionless parameters [33]:

$$\nabla^* = L\nabla\ ,\ T^* = \frac{T - T_c}{T_H - T_C}\ ,\ \boldsymbol{V}^* = \frac{\boldsymbol{V}L}{v_f}\ ,\ P^* = \frac{PL^2}{\rho_f v_f^2}, \boldsymbol{B}^* = \frac{\boldsymbol{B}}{B_0},\ \phi^* = \frac{\phi}{\phi_{Ave}}\ ,$$

$$\delta = \frac{T_c}{\Delta T}\ ,\ D_B^* = \frac{D_B}{D_{B0}}\ ,\ D_T^* = \frac{D_T}{D_{T0}},\ D_{B0} = \frac{K_B T_c}{3\pi\mu_f d_{np}},\ D_{T0} = \gamma\frac{\mu_f}{\rho_f}\phi_{Ave}$$

Continuity equation [34]:

$$\nabla^* .\boldsymbol{V}^* = 0. \tag{1}$$

momentum equation:

$$\left(\frac{\rho_{nf}}{\rho_f}\right)(\boldsymbol{V}^*.\nabla^*)\boldsymbol{V}^* = -\nabla^* P^* + \nabla^*.\left(\frac{\mu_{nf}}{\mu_f}\nabla^*\boldsymbol{V}^*\right) + \left(\frac{(\rho\beta)_{nf}}{\rho_f\beta_f}\right)\frac{Ra_f}{Pr}T^*.\hat{\boldsymbol{e}}_{\boldsymbol{g}} - Ha^2(\boldsymbol{V}^*\times\boldsymbol{B}^*)\times\boldsymbol{B}^*. \tag{2}$$

Energy equation [35]:

$$\frac{(\rho C_P)_{nf}}{(\rho C_P)_f}\boldsymbol{V}^*.\nabla^* T^* = \frac{1}{Pr}\nabla^*\left(\frac{k_{nf}}{k_f}\nabla^* T^*\right) + \frac{1}{Pr}\frac{1}{Le}\left(D_B^*\nabla^*\phi^*.\nabla^* T^* + \frac{D_T^*}{N_{BT}}\frac{\nabla^* T^*.\nabla^* T^*}{1 + T^*/\delta}\right) \tag{3}$$

Mass transfer equation:

The Buongiorno model is considered mechanisms of Brownian and Thermophoresis motion [35].

$$\boldsymbol{V}^*.\nabla^*\phi^* = \frac{1}{Sc}\nabla^*.\left(D_B^*\nabla^*\phi^* + \frac{D_T^*}{N_{BT}}\frac{\nabla^* T^*}{1 + T^*/\delta}\right) \tag{4}$$

The dimensionless numbers that appear are as follows:

$$Pr = \frac{v_f}{\alpha_f},\ Ra = \frac{g\beta_f\Delta T L^3}{\alpha_f v_f},\ Ha = B_0 L\sqrt{\frac{\sigma_f}{\mu_f}},\ Le = \frac{k_f}{(\rho C_p)_{np} D_{B0}\phi_{Ave}},\ N_{BT} = \frac{\phi_{Ave} D_{B0}\delta}{D_{T0}},\ Sc = \frac{v_f}{D_{B0}}$$

Which $Pr,\ Ra,\ Ha,\ Le,\ Sc,\ and\ N_{BT}$ are Prandtl, Rayleigh, Hartman, Lewis, Schmitt number, and ratio of Brownian to thermophoresis diffusivity, respectively [36–38].

We can calculate average Nusselt number of on wall cylinder as follow:

$$Nu_{Ave} = \frac{1}{A}\oint\nabla^* T^*.ds$$

Which A and s is element and cylinder areas.

1.3. Properties of nanofluids

The thermophysical properties of water-Cu nanofluid such as: density, dynamic viscosity, thermal conductivity, heat capacity, coefficient of thermal expansion, and electrical conductivity, respectively [39].

$$\rho_{nf} = (1-\phi)\rho_f + \phi\rho_{np} \tag{5}$$

$$\mu_{nf} = \frac{\mu_f}{(1-\phi)^{2.5}} \tag{6}$$

Table 1
Thermophysical properties of water, and Cu nanoparticles [40].

	$\rho\left(\frac{kg}{m^3}\right)$	$k\left(\frac{W}{mK}\right)$	$C_p\left(\frac{J}{kgK}\right)$	$\beta\times 10^{-5}\left(\frac{1}{K}\right)$	$\mu\times 10^{-6}\left(\frac{kg}{ms}\right)$	$d_p(nm)$	$\sigma(1/\Omega.m)$
water	993	0.628	4178	36.2	695	0.384	0.05
Cu	8933	401	385	1.67	–	30	5.96×10^7

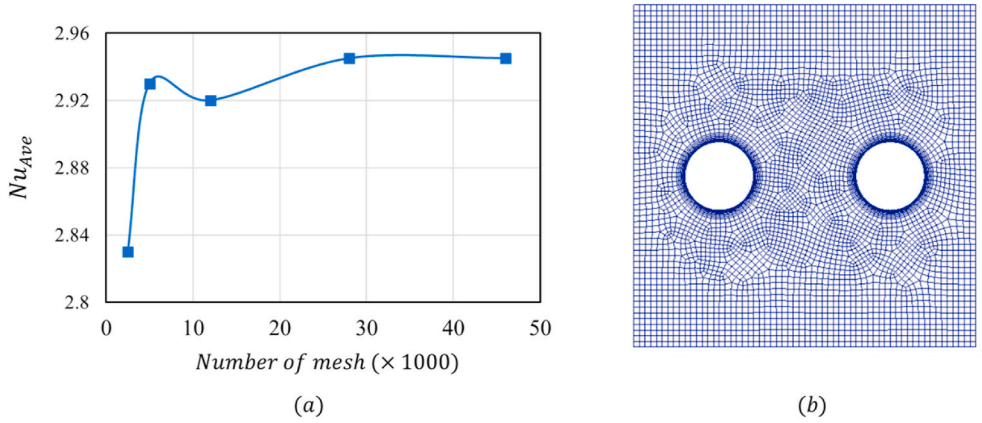

Fig. 2. (a) Mesh sensitivity curve for two-phase Nusselt number and (b) the used mesh for present simulation.

$$\frac{k_{nf}}{k_f}=\frac{k_{np}+2k_f+2\phi\left(k_{np}-k_f\right)}{k_{np}+2k_f-\phi\left(k_{np}-k_f\right)} \tag{7}$$

$$(\rho C_P)_{nf}=(1-\phi)\left(\rho C_p\right)_f+\phi(\rho C_P)_{np} \tag{8}$$

$$(\rho\beta)_{nf}=(1-\phi)(\rho\beta)_f+\phi(\rho\beta)_{np} \tag{9}$$

$$\sigma_{nf}=\sigma_f\left[1+\frac{3\left(\sigma_{np}/\sigma_f-1\right)\phi}{\left(\sigma_{np}/\sigma_f+2\right)-\left(\sigma_{np}/\sigma_f-1\right)\phi}\right]. \tag{10}$$

The thermophysical properties of water and copper nanoparticles are as shown in Table 1.
To solve the coupled equations, the boundary conditions on the cavity and pipes walls are as follows:
On the cavity walls:

$$\boldsymbol{V}^*=0,\nabla^*T^*.\boldsymbol{n}=0,\ \text{and}\ \nabla^*\phi^*.\boldsymbol{n}=0. \tag{11}$$

On the hot pipe wall:

$$\boldsymbol{V}^*=0,\ T^*=1\ ,\ \text{and}\ \nabla^*\phi^*.n=-\frac{1}{D_B^*}\frac{D_T^*}{N_{BT}}\frac{\nabla^*T^*}{1+T^*/_\delta} \tag{12}$$

On the cold pipe wall:

$$\boldsymbol{V}^*=0,\ T^*=0,\ \text{and}\ \nabla^*\phi^*.n=-\frac{1}{D_B^*}\frac{D_T^*}{N_{BT}}\frac{\nabla^*T^*}{1+T^*/_\delta} \tag{13}$$

In the above equations, $\boldsymbol{n}$ denotes the unit vector that is normal to the boundary.

1.4. Numerical settings and independence of mesh

In this study, relying on numerical solutions and methods in computational fluid dynamics (CFD), the hypotheses under discussion are implemented [41and42]. As the hypotheses became more complex, attempts were made to exploit them using open source and extensible software [43and44]. In this study, the aim is to implement computational fluid dynamics. For the present study, the developed C++ code is used to simulate the MHD natural convection of water-Cu nanofluid inside a cavity. The finite volume method with SIMPLE algorithm is applied for velocity and pressure coupling with relaxation factor of 0.5. Moreover, the first-order upwind and central scheme with accuracy of second order are implemented to discretize convective and diffusive terms in PDEs equation and

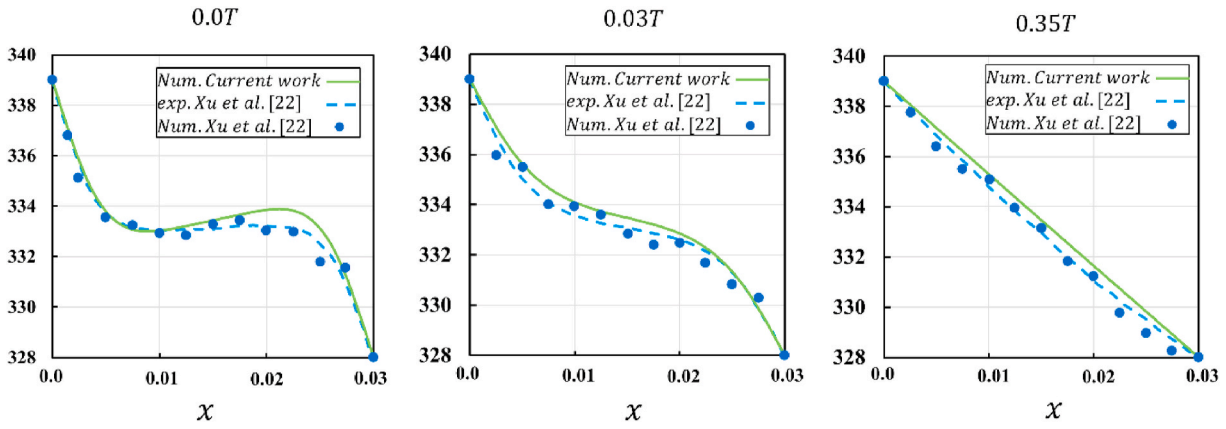

Fig. 3. Results of temperature distribution in the line y = 1.5 cm for different magnetic field intensitiy between the present work and the study [18].

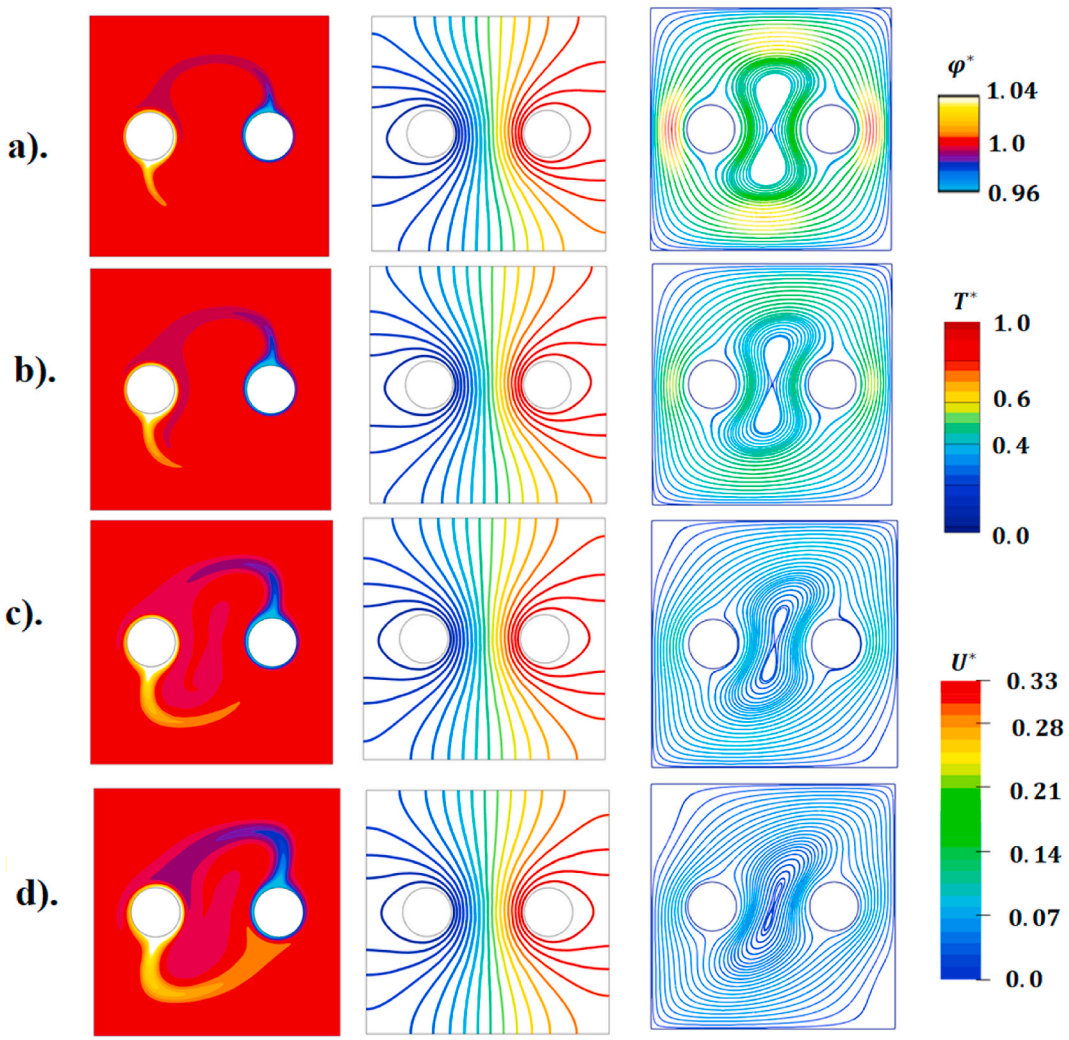

Fig. 4. The volume fraction contours, isothermal lines, and streamlines from left to right, respectively. For $Ra = 10^3$, $\phi_{Ave} = 0.02$, *and* $\eta =$ 30at *a*). $Ha = 0$, *b*). $Ha = 15$, *c*). $Ha = 30$, *and d*). $Ha = 45$.

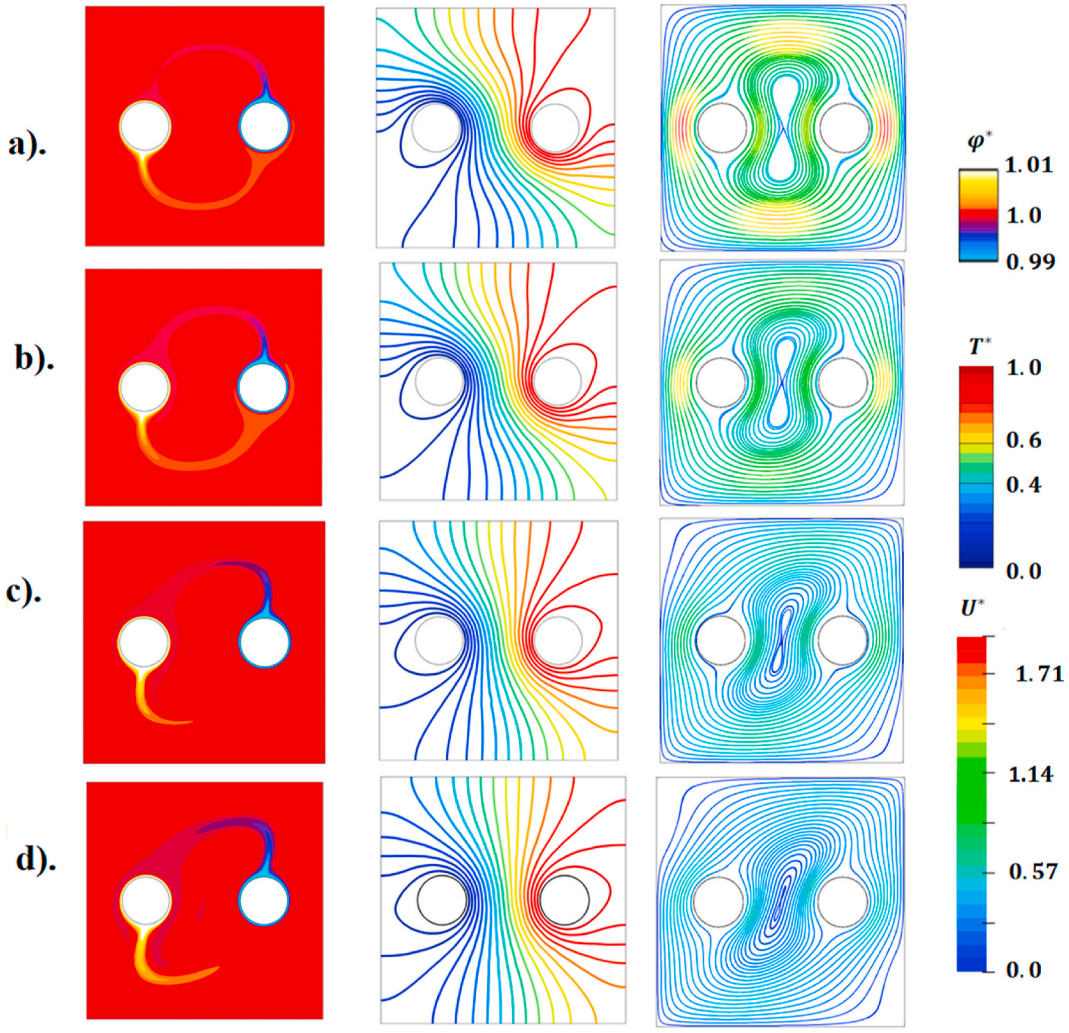

Fig. 5. The volume fraction contours, isothermal lines, and streamlines from left to right, respectively. For $Ra = 10^4$, $\phi_{Ave} = 0.02$, *and* $\eta = 30$at *a*). $Ha = 0$, *b*). $Ha = 15$, *c*). $Ha = 30$, *and d*). $Ha = 45$.

boundary condition. Mesh gradient is used near the HACs and unstructured mesh is used inside cavity. Also, the sensitivity of the two-phase Nusselt to the mesh and used mesh (Fig. 2) is studied for the critical conditions: $Ra = 10^3$, $Ha = 45$, $\phi_{Ave} = 0.04$, $\eta = 0$. Nusselt values differ by less than one percent from 12k to 28k mesh and remain constant from 28k to 46k mesh. In this simulation, 46k mesh is selected for other cases.

1.5. Validation

To validate the developed code, the study [18] investigated the free convection of molten gallium in the presence of a uniform magnetic field inside a cavity numerically and experimentally. According to Fig. 3, results of research [18] and current work are compared for temperature distribution in the y = 1.5 cm line in different values of magnetic field intensity. the results are in good agreement.

2. Results and discussion

In the present study, we investigated the volume fraction counters, isothermal lines, flow patterns, and Nusselt numbers. The results for $Ra = 10^3 - 10^5$ and $0 \leq \phi_{Ave} \leq 0.04$are also given for different inclination angles of enclosure ($0 \leq \eta \leq 90$) and different Hartmann numbers, which represent the magnetic field strength (Ha = 0–45). The effects of each of mentioned parameters are investigated separately in different sections.

Evaluation and analysis of the effects of MHD magnetic field and Rayleigh number are given in Figs. 4–6. Each figure is illustrated at $\phi_{Ave} = 0.02$ and $\eta = 30^o$. Fig. 4 shows the volume fraction contours, isothermal lines, and streamlines from left to right, respectively.

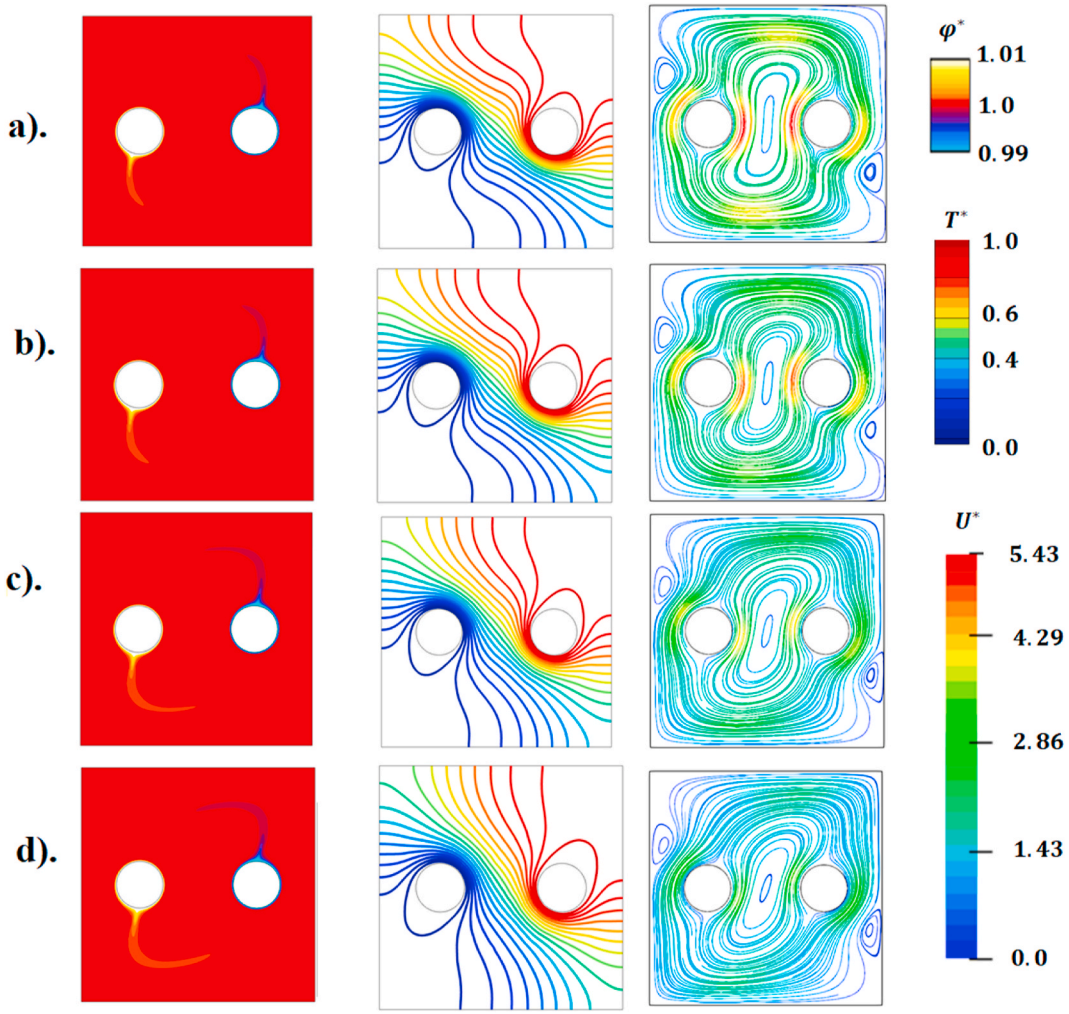

Fig. 6. The volume fraction contours, isothermal lines, and streamlines from left to right, respectively. For $Ra = 10^5$, $\phi_{Ave} = 0.02$, *and* $\eta = 30$at *a*). $Ha = 0$, *b*). $Ha = 15$, *c*). $Ha = 30$, *and d*). $Ha = 45$.

According to the form of isothermal lines, it is observed that the conduction heat transfer mechanism is dominant. The flow pattern consists of two vortices. The middle vortex is spindle-shaped and the large vortex is in the shape of concentric circles.

As shown in Fig. 1 the right cylinder is at a high constant temperature and the left cylinder has a lower temperature. Therefore, in the volume fraction contours of Fig. 4, the nanoparticles move towards the low-temperature cylinder on the high-temperature cylinder. This is due to the effects of thermophoresis. Based on this phenomenon, nanoparticles are thrown from the hot wall to the cold wall due to the temperature gradient.

As the Ha number increases (Fig. 4), the streamlines deviate from the state of concentric circles and become elliptical. The middle spindle vortex is also oblique. In other word, intensifying the magnetic field has reduced the flow velocity. Since the predominant mechanism of heat transfer is conduction. There is not much change in isothermal lines. By increasing Ha number, the distribution of nanoparticles has become very non-uniform. This is because the flow velocity is reduced. As a result, the diffusion of nanoparticles becoming important.

Fig. 5 shows the same results as Fig. 4, this time for $Ra = 10^4$. In this Ra number, the increase in Ha number has also caused the streamlines to deviate. In other words, applying a magnetic field to the fluid flow causes resistance to the movement of the fluid, which also slows down the velocity of the flow. The resistance created in isothermal lines is also noticeable. As the Ha number increases further, the isothermal lines become such as isothermal lines of pure conduction. According to the velocity decreases, the density of nanoparticles increases.

Fig. 6 illustrates the streamlines, isothermal lines, and volume fraction contours at $Ra = 10^5$. Two small vortices have appeared on the sides of the enclosure. In the presence of small vortices, the temperature gradient intensifies and the isothermal lines approach each other. Also, the presence of small vortices has increased the heat transfer mechanism of the convection. Hence the form of isothermal lines is very different from the isothermal lines of pure conduction. In the same Ra number, the application of a magnetic field to the

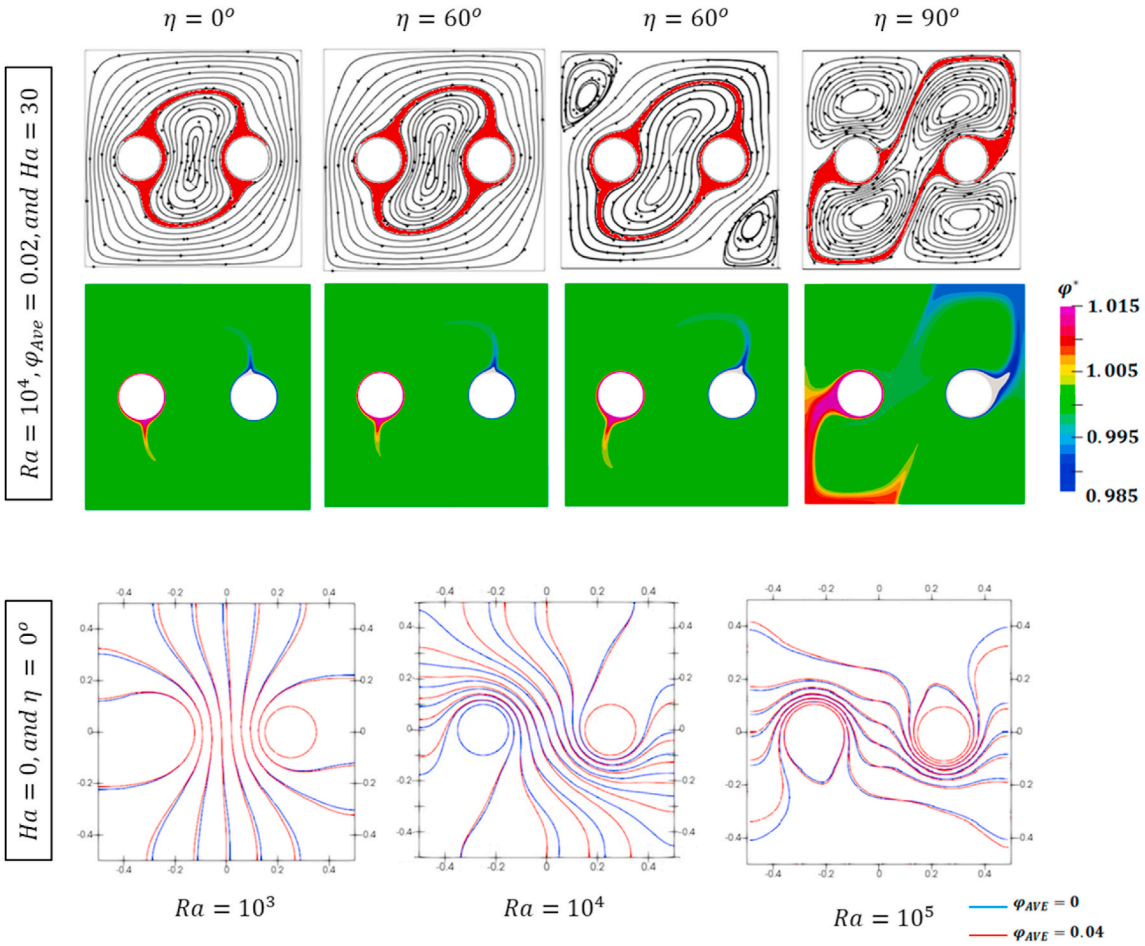

Fig. 7. Flow pattern (first row) and nanoparticle distribution counters (second row) for $Ra = 10^4$, $\phi_{Ave} = 0.02$, *and* $Ha = 30$, and isothermal lines (third row) for Ha = 0, $\eta = 0^o$.

fluid flow reduces the velocity of the flow. The resistance created in the isothermal lines is also felt. And with increasing Ha number, the density of isothermal lines decreased. As the velocity decreases, the inhomogeneous concentration of nanoparticles increases.

The effect of the presence of a magnetic field in three different Ra numbers evaluated. Here, we are going to evaluate the effect of the Ra number by comparing Figs. 4–6. In the first place, by comparing the dimensionless velocity at different Ra numbers, it is observed that with increasing the Ra number, the flow velocity has increased significantly. So that in $Ra = 10^5$ we see the emergence of two more vortices. With increasing velocity, convection heat transfer has prevailed. Which has affected the isothermal lines and the distortion of these lines has increased. Also, isothermal lines near the cylinders are condensed. The increase in velocity at high Ra numbers also caused the nanoparticles to disperse evenly. The maximum ϕ^* decreased from 1.04 at $Ra = 10^3$ to 1.01 at $Ra = 10^5$.

Fig. 7, first and second rows depicts the flow patterns with volume fraction contours for different inclination angles (η). The aim of this section is to analyze the effects of inclination angle of enclosure on the accumulation of nanoparticles and the flow pattern. In each of the flow patterns, areas are shown in red color. These areas are responsible for transporting nanoparticles. Due to the fact that when the flow approaches the cylinder, the flow velocity in the area of collision with the cylinder (Stagnation point) is equal to zero. Also, the velocity at the rear of the cylinder is also greatly reduced. Hence, the red zone in all diagrams has a low velocity. The low velocity in these regions causes diffusion and non-uniform dispersion of nanoparticles. This is evident in the line of volume fraction contours of nanoparticles. The nanoparticles are thrown from the hot cylinder to the cold cylinder. In other areas, due to the higher flow rate and low temperature gradient, the nanoparticles are evenly distributed.

In Fig. 7, the flow pattern changes completely with increasing inclination angle. As far as $\eta = 90^o$ we see the creation of four large vortices. By turning more enclosure velocity decreases (not presented here). As the flow rate decreases, the non-uniform diffusion rate of the nanoparticles increases. At an angle of $\eta = 90^o$, as the nanoparticle transfer zone gets closer to the outer walls, this region grows and the effects of the no-slip condition of the side walls also contribute to the stagnation point effects, resulting in more area being involved. Hence at $\eta = 90^o$, the nanoparticle concentration is much more non-uniform.

Third row of Fig. 7 presents the isothermal lines in different Ra numbers for two volume fractions of zero and 0.04. In the lower Ra numbers, the conduction is predominant. Adding the nanoparticles does not have a specific effect on isothermal lines, but with

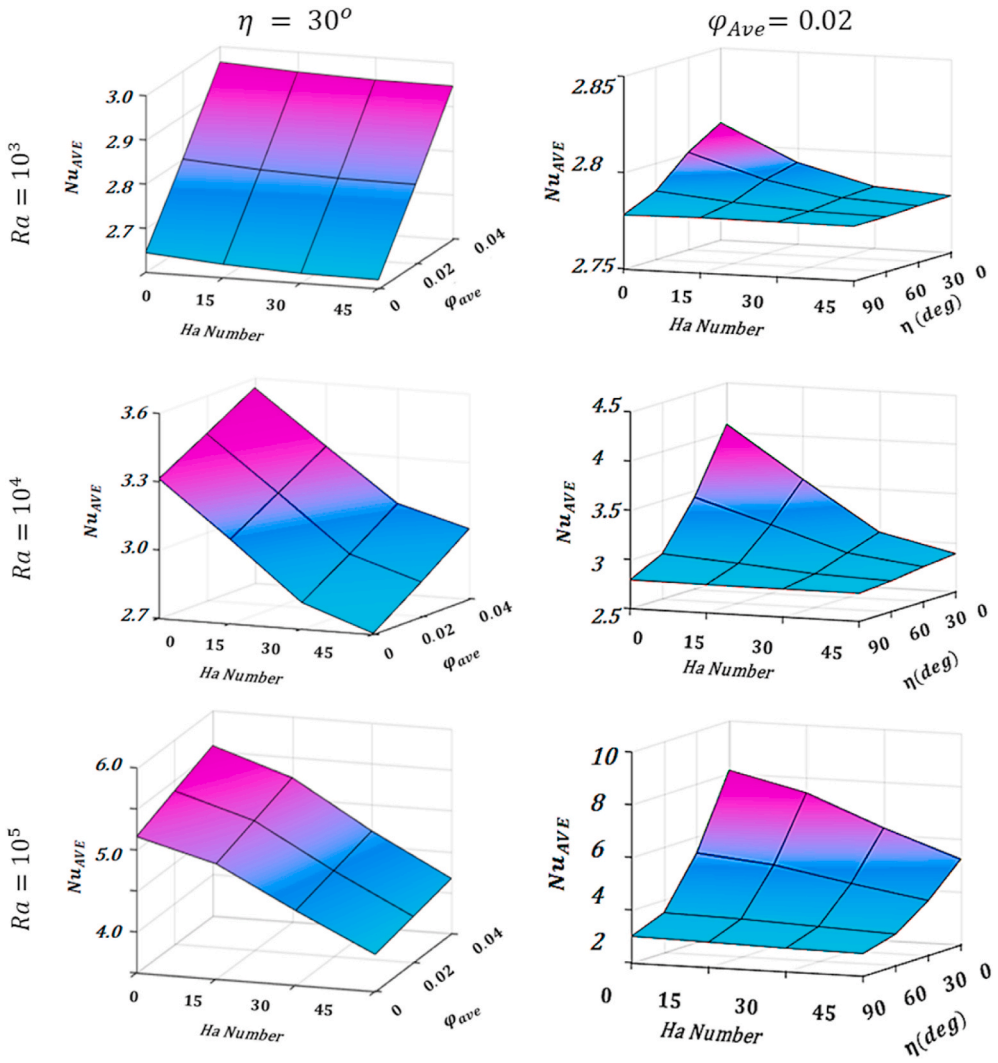

Fig. 8. Average Nusselt number on hot cylinder at $\eta = 30^o$(first column) for different Ha numbers and volume fractions, and $\phi_{Ave} = 0.02$ (second column) for different Ha numbers and inclination angles.

increasing Ra number and convection prevailing, the effects of volume fraction have become more pronounced. To better understand the effects of volume fraction on heat transfer, Fig. 8 is presented.

Fig. 8 shows the average Nusselt number for different volume fractions and Ha numbers in three different Ra numbers. $Nu_{A\ VE}$ improves with adding nanoparticles. This improvement can be seen in all three Ra numbers. Due to the low flow rate at the low Ra number, intensifying the magnetic field at $Ra = 10^3$ does not have a significant effect on the $Nu_{A\ VE}$, and only a very small amount reduces it. As a result, the presence of a magnetic field creates less resistance to fluid motion. With increasing Ra number $Nu_{A\ VE}$ has increased (compared to $Ra = 10^3$). This increase is greater in the high volume fraction. At the high Ra number, the presence of a magnetic field has a significant effect on the heat transfer rate. The $Nu_{A\ VE}$decreases at Ha = 30 but when the $Nu_{A\ VE}$ is sufficiently low (close to the $Nu_{A\ VE}$ values at $Ra = 10^3$) the field has less effect on $Nu_{A\ VE}$. As the Ra number increases further, the Nusselt values become much larger, and the increase in volume fraction increases the $Nu_{A\ VE}$, and the Ha number is inversely related to the $Nu_{A\ VE}$.

$Nu_{A\ VE}$ for investigating the inclination angle of enclosure (η) in different Ha and Ra numbers are shown in Fig. 8. At $Ra = 10^3$ the $Nu_{A\ VE}$ decreases with increasing η. Making enclosure more horizontal causes the higher the $Nu_{A\ VE}$ and the greater the effect of the Ha number. However, at higher η, the effects of the magnetic field are much less noticeable. At $Ra = 10^4$, the effect of η is very strong and with increasing η it accepts less effect of the presence of the magnetic field. However, with increasing Rayleigh number (Fig. 8), the effect of heat transfer rate from the magnetic field (unlike the previous two Ra numbers) is less and decreases at $\eta = 0$ with a smaller slope. At $Ra = 10^4$, $Nu_{A\ VE}$ is greatly reduced at $\eta = 90^o$ and is not affected by the Ha number.

By comparing Fig. 8, it can be seen that the Ra number has the greatest effect on the heat transfer rate. The second parameter in terms of effectiveness is η. In other words, the inclination angle has a significant effect on how the magnetic field or volume fraction

affects. The effect of the Ha number is similar to the η and is almost as important. Finally, the volume fraction of nanoparticles has a positive effect on the heat transfer rate, so that in the lower Ra number, the effects of the volume fraction of nanoparticles are more pronounced than the magnetic field.

3. Conclusion

A heat exchanger consisting of a constant-temperature hot cylinder and a cold cylinder was evaluated for being in a square enclosure in the presence of nanoparticles. The modeling was performed in two dimensions and the effects of the inclination angle of enclosure (η) and the magnetic field were evaluated under MHD conditions. The following results can be extracted by analysis and studies:

One area in the study was observed in which nanoparticles were distributed unevenly and was termed the nanoparticle transfer zone. Clearly, the diffusion effects of thermophoresis were very pronounced in this area. In this way, the nanoparticles were moved from the hot cylinder inside the zone to the cold cylinder. Evaluations showed that the application of a magnetic field causes the nanoparticle transport area to be enlarged and the nanoparticles to be distributed more unevenly inside the enclosure. As the inclination angle of the enclosure increased, the zone grew and the distribution of nanoparticles became more non-uniform. However, the increase in Ra number and consequently the convection effects caused them to be homogeneously distributed inside the enclosure.

In general, increasing the Rayleigh number and volume fraction of nanoparticles improved the heat transfer rate. Applying and intensifying the magnetic field reduced the heat transfer rate. Especially at low Ra numbers and high η the effects of the presence of a magnetic field were very small. Increasing the η reduced the heat transfer rate. This effect was much more noticeable in the higher Ra number.

Author statement

Yan Cao: Supervision, Conceptualization. Hamdi Ayed: Validation, Funding acquisition. Fahd Jarad: Data Curation, Software. Hussein Togun: Writing - Review & Editing, Data Curation. Hajar Alias: Visualization, Investigation. Alibek Issakhov: Writing - Original Draft. Mahidzal Dahari: Writing - Review & Editing, Funding acquisition. Makatar Wae-hayee: Project administration, Formal analysis. Mohamed Hechmi El Ouni: Visualization, Resources.

Declaration of competing interest

The authors declare that they have no known competing financial interests or personal relationships that could have appeared to influence the work reported in this paper.

Acknowledgment

The authors acknowledge the Deanship of Scientific Research for providing administrative and financial support. Funding for this work has been provided by the Deanship of Scientific Research, King Khalid University, Ministry of Education, Kingdom of Saudi Arabia, under research grant award number RGP. 2/100/42." and by Universiti Malaya under grant No. GPF054A-2020. Also, the authors would like to express our gratitude to Universiti Teknologi Malaysia for giving the Fellow Research Grant to Dr Hussein Togun (Vot. No R.J130000.7113.00P12)

References

[1] Chao Liu, Mehran Hashemian, Shawabkeh Ali, S. Hamed Sadighi Dizaji, M.F. Saleem, B. Mohideen, MakatarWae-hayee, CFD-based irreversibility analysis of avant-garde semi-O/O-shape grooving fashions of solar pond heat trade-off unit, Renew. Energy 171 (2021) 328–343.

[2] Y. Cao, H. Ayed, H. Sadighi Dizaji, M. Hashemian, M. Wae-hayee, Entropic analysis of a double helical tube heat exchanger including circular depressions on both inner and outer tube, Case Studies in Thermal Engineering 26 (2021), 101053.

[3] Z. Ni, X. Cao, X. Wang, S. Zhou, C. Zhang, B. Xu, Y. Ni, Facile synthesis of copper (I) oxide nanochains and the photo-thermal conversion performance of its nanofluids, Coatings 11 (7) (2021) 749.

[4] Y. Wang, C. Li, Y. Zhang, M. Yang, B. Li, D. Jia, Y. Hou, C. Mao, Experimental evaluation of the lubrication properties of the wheel/workpiece interface in minimum quantity lubrication (MQL) grinding using different types of vegetable oils, J. Clean. Prod. 127 (2016) 487–499.

[5] Yanbin Zhang, L.I. Hao Nan, L.I. Changhe, Chuanzhen Huang, A.L.I. Hafiz Muhammad, X.U. Xuefeng, M.A.O. Cong, D.I.N.G. Wenfeng, C.U.I. Xin, Y.A.N.G. Min, Y.U. Tianbiao, J.A.M.I.L. Muhammad, Munish Kumar Gupta, Dongzhou Jia, S.A.I.D. Zafar, Nano-enhanced biolubricant in sustainable manufacturing: from processability to mechanisms, Friction (2021), https://doi.org/10.1007/s40544-021-0536-y. Press.

[6] C. Shi, X. Zhang, X. Zhang, P. Chen, L. Xu, Ultrasonic desulfurization of amphiphilic magnetic-Janus nanosheets in oil-water mixture system, Ultrason. Sonochem. 76 (2021), 105662.

[7] F. Garoosi, G. Bagheri, F. Talebi, Numerical simulation of natural convection of nanofluids in a square cavity with several pairs of heaters and coolers (HACs) inside, Int. J. Heat Mass Tran. 67 (2013) 362–376.

[8] Yan Cao, Hamdi Ayed, Mehran Hashemian, Alibek Issakhov, Makatar Wae-hayee, Thermal/frictional performance of spiral pipe with ring-shape depression used as in-pond heat exchanger, Sol. Energy 224 (2021) 742–756, https://doi.org/10.1016/j.solener.2021.06.039.

[9] X. Duan, B. Deng, Y. Liu, Y. Li, J. Liu, Experimental study the impacts of the key operating and design parameters on the cycle-to-cycle variations of the natural gas SI engine, Fuel 290 (2021), 119976.

[10] N. Zhao, L. Deng, D. Luo, P. Zhang, One-step fabrication of biomass-derived hierarchically porous carbon/MnO nanosheets composites for symmetric hybrid supercapacitor, Appl. Surf. Sci. 526 (2020), 146696.

[11] X. Zhang, X. Sun, T. Lv, L. Weng, M. Chi, J. Shi, S. Zhang, Preparation of PI porous fiber membrane for recovering oil-paper insulation structure, J. Mater. Sci. Mater. Electron. 31 (16) (2020) 13344–13351.

[12] F. Garoosi, F. Hoseininejad, M.M. Rashidi, Numerical study of natural convection heat transfer in a heat exchanger filled with nanofluids, Energy 109 (2016) 664–678.
[13] Yusuf A. Al-Turki, Hazim Moria, Ali Shawabkeh, Samira Pourhedayat, Mehran Hashemian, Hamed Sadighi Dizaji, Thermal, frictional and exergetic analysis of non-parallel configurations for plate heat exchangers, Chemical Engineering and Processing - Process Intensification 161 (2021), 108319.
[14] H. Cheng, T. Li, X. Li, J. Feng, T. Tang, D. Qin, Facile synthesis of Co9S8 nanocages as an electrochemical sensor for luteolin detection, J. Electrochem. Soc. 168 (8) (2021), 087504.
[15] S. Pourhedayat, S.M. Pesteei, H.E. Ghalinghie, M. Hashemian, M.A. Ashraf, Thermal-exergetic behavior of triangular vortex generators through the cylindrical tubes, Int. J. Heat Mass Tran. 151 (2020), 119406.
[16] R. Ye, P. Liu, K. Shi, B. Yan, State damping control: a novel simple method of Rotor UAV with high performance, IEEE Access 8 (2020) 214346–214357.
[17] S.E. Ahmed, M.A. Mansour, A.M. Rashad, T. Salah, MHD natural convection from two heating modes in fined triangular enclosures filled with porous media using nanofluids, J. Therm. Anal. Calorim. 139 (5) (2020) 3133–3149.
[18] M.D. Massoudi, M.B.B. Hamida, MHD natural convection and thermal radiation of diamond–water nanofluid around rotating elliptical baffle inside inclined trapezoidal cavity, The European Physical Journal Plus 135 (11) (2020) 1–24.
[19] J. Buongiorno, Convective Transport in Nanofluids, 2006.
[20] A. Alhashash, Natural convection of nanoliquid from a cylinder in square porous enclosure using Buongiorno's two-phase model, Sci. Rep. 10 (1) (2020) 1–12.
[21] G.A. Sheikhzadeh, M. Dastmalchi, H. Khorasanizadeh, Effects of nanoparticles transport mechanisms on Al2O 3-water nanofluid natural convection in a square enclosure, Int. J. Therm. Sci. 66 (2013) 51–62, https://doi.org/10.1016/j.ijthermalsci.2012.12.001.
[22] Mohammad Jalili, Ata Chitsaz, Mehran Hashemian, Marc A. Rosen, Economic and environmental assessment using emergy of a geothermal power plant, Energy Convers. Manag. 228 (2021), 113666, https://doi.org/10.1016/j.enconman.2020.113666.
[23] Samira Pourhedayat, Seyed Mehdi Pesteei, Hamed Ebrahimi Ghalinghie, Mehran Hashemian, Muhammad Aqeel Ashraf, Thermal-exergetic behavior of triangular vortex generators through the cylindrical tubes, Int. J. Heat Mass Tran. 151 (2020), 119406, https://doi.org/10.1016/j.ijheatmasstransfer.2020.119406.
[24] Mingzheng Liu, Changhe Li, Yanbin Zhang, Qinglong An, Min Yang, Teng Gao, Cong Mao, Bo Liu, Huajun Cao, Xuefeng Xu, Zafar Said, Sujan Debnath, Muhammad Jamil, Hafz Muhammad Ali, Shubham Sharma, Cryogenic minimum quantity lubrication machining: from mechanism to application, Front. Mech. Eng. (2021), https://doi.org/10.1007/s11465-021-0654-2 in press.
[25] Shirko Jafary, Shahram Khalilarya, Ali Shawabkeh, Makatar Wae-hayee, Mehran Hashemian, A complete energetic and exergetic analysis of a solar powered trigeneration system with two novel organic Rankine cycle (ORC) configurations, J. Clean. Prod. 281 (2021), 124552, https://doi.org/10.1016/j.jclepro.2020.124552.
[26] F. Garoosi, L. Jahanshaloo, M.M. Rashidi, A. Badakhsh, M.E. Ali, Numerical simulation of natural convection of the nanofluid in heat exchangers using a Buongiorno model, Appl. Math. Comput. 254 (2015) 183–203.
[27] A.I. Alsabery, M.A. Sheremet, A.J. Chamkha, I. Hashim, Conjugate natural convection of Al2O3–water nanofluid in a square cavity with a concentric solid insert using Buongiorno's two-phase model, Int. J. Mech. Sci. 136 (2018) 200–219.
[28] I. Hashim, A.I. Alsabery, M.A. Sheremet, A.J. Chamkha, Numerical investigation of natural convection of Al2O3-water nanofluid in a wavy cavity with conductive inner block using Buongiorno's two-phase model, Adv. Powder Technol. 30 (2) (2019) 399–414.
[29] N.S. Bondareva, M.A. Sheremet, I. Pop, Magnetic field effect on the unsteady natural convection in a right-angle trapezoidal cavity filled with a nanofluid: Buongiorno's mathematical model, Int. J. Numer. Methods Heat Fluid Flow 25 (8) (2015) 1924–1946 (23).
[30] M.A. Sheremet, I. Pop, N.C. Roşca, Magnetic field effect on the unsteady natural convection in a wavy-walled cavity filled with a nanofluid: Buongiorno's mathematical model, Journal of the Taiwan Institute of Chemical Engineers 61 (2016) 211–222.
[31] M. Mahmoodi, S.M. Sebdani, Natural convection in a square cavity containing a nanofluid and an adiabatic square block at the center, Superlattice. Microst. 52 (2) (2012) 261–275.
[32] S.Y. Motlagh, E. Golab, A.N. Sadr, Two-phase modeling of the free convection of nanofluid inside the inclined porous semi-annulus enclosure, Int. J. Mech. Sci. 164 (2019), 105183.
[33] S. Goudarzi, M. Shekaramiz, A. Omidvar, E. Golab, A. Karimipour, A. Karimipour, Nanoparticles migration due to thermophoresis and Brownian motion and its impact on Ag-MgO/Water hybrid nanofluid natural convection, Powder Technol. 375 (2020) 493–503.
[34] M. Abbasi, Wall Shear Stress Vector Field Topology Characterization Using 4D-Flow MRI, 2020.
[35] M. Abbasi, A.N. Esfahani, E. Golab, O. Golestanian, N. Ashouri, S.M. Sajadi, F. Ghaemi, D. Baleanu, A. Karimipour, Effects of Brownian motions and thermophoresis diffusions on the hematocrit and LDL concentration/diameter of pulsatile non-Newtonian blood in abdominal aortic aneurysm, J. Non-Newtonian Fluid Mech. (2021), 104576.
[36] E. Golab, S. Goudarzi, H. Kazemi-Varnamkhasti, H. Amigh, F. Ghaemi, D. Baleanu, A. Karimipour, Investigation of the effect of adding nano-encapsulated phase change material to water in natural convection inside a rectangular cavity, Journal of Energy Storage 40 (2021), 102699.
[37] Shu-RongYan, Hazim Moria, Samira Pourhedayat, Mehran Hashemian, Soheil Asaadi, Hamed Sadighi Dizaji, Kittisak Jermsittiparsert, A critique of effectiveness concept for heat exchangers; theoretical-experimental study, Int. J. Heat Mass Tran. 159 (2020) 120160.
[38] Yan Cao, Hamdi Ayed, Samad Jafarmadar, Mir Ali Asghar Abdollahi, Farag Ahmed, Makatar Wae-hayee, Mehran Hashemian, PEM fuel cell cathode-side flow field design optimization based on multi-criteria analysis of liquid-slug dynamics, J. Ind. Eng. Chem. 98 (2021) 397–412, https://doi.org/10.1016/j.jiec.2021.03.024.
[39] M. Shekaramiz, S. Fathi, H.A. Ataabadi, H. Kazemi-Varnamkhasti, D. Toghraie, MHD nanofluid free convection inside the wavy triangular cavity considering periodic temperature boundary condition and velocity slip mechanisms, Int. J. Therm. Sci. 170 (2021), 107179.
[40] M. Izadi, G. Hoghoughi, R. Mohebbi, M. Sheremet, Nanoparticle migration and natural convection heat transfer of Cu-water nanofluid inside a porous undulant-wall enclosure using LTNE and two-phase model, J. Mol. Liq. 261 (2018) 357–372.
[41] M. Habibi, S. Dawson, A. Arzani, Data-driven pulsatile blood flow physics with dynamic mode decomposition, Fluid 5 (3) (2020) 111.
[42] M. Habibi, Data-Driven and Multi-Modality Modeling of Blood Flow Physics, Doctoral dissertation, Northern Arizona University, 2021.
[43] M. Habibi, R. D'Souza, S. Dawson, A. Arzani, Hemodynamic data assimilation using model order reduction and Kalman filter, in: APS Division of Fluid Dynamics Meeting Abstracts, 2020. W09-003.
[44] M. Habibi, S. Dawson, A. Arzani, Reduced order modeling of pulsatile blood flow: multistage dynamic mode decomposition with control, in: APS Division of Fluid Dynamics Meeting Abstracts, 2019, November, pp. Q29–Q2009.